Wind and Structures, Vol. 6, No. 3 (2003) 221-248
DOI: http://dx.doi.org/10.12989/was.2003.6.3.221

Design of tall residential buildings in Singapore for wind effects

T. Balendra[†] and Z. Ma[‡]

Department of Civil Engineering, National University of Singapore, Block E1A, #07-03, Engineering Drive 2, Singapore 117576, Singapore

C. L. Tan[‡†]

Structural Engineering Department, Housing & Development Board, 480 Lorong 6 Toa Payoh, Singapore 310480, Singapore

(Received September 23, 2002, Accepted April 29, 2003)

Abstract. The design of high-rise building is often influenced by wind-induced motions such as accelerations and lateral deflections. Consequently, the building's structural stiffness and dynamic (vibration periods and damping) properties become important parameters in the determination of such motions. The approximate methods and empirical expressions used to quantify these parameters at the design phase tend to yield values significantly different from each other. In view of this, there is a need to examine how actual buildings in the field respond to dynamic wind loading in order to ascertain a more realistic model for the dynamic behavior of buildings. This paper describes the findings from full-scale measurements of the wind-induced response of typical high-rise buildings in Singapore, and recommends an empirical forecast model for periods of vibration of typical buildings in Singapore, an appropriate computer model for determining the periods of vibration, and appropriate expressions which relate the wind speed to accelerations in buildings based on wind tunnel force balance model test and field results.

Key words: field measurements; tall buildings; wind induced acceleration; wind loads; force balance test.

1. Introduction

Modern high-rise buildings are constructed with higher-grade concrete and light-weight materials and are therefore more flexible and lightly damped compared to their predecessors. As a result, these buildings are more sensitive towards wind-induced excitation. Of particular interests are the accelerations and lateral deflections which govern the design, as the buildings get taller.

A building's structural stiffness and dynamic properties such as periods, mode shapes and damping are needed to ascertain its response under lateral loading. However, correct estimation of these parameters is generally difficult as there are a great deal of uncertainty involved. For instance, the building's stiffness is frequently assumed to be due to the structural elements and the

† Associate Professor
‡ Research Scholar
‡† Executive Structural Engineer

contributions from the non-structural components such as internal partitions and external brick walls, are usually and conveniently ignored. Though difficult to quantify, these partitions contribute a fair share to the overall rigidity and to disregard them completely would clearly underestimate the building's lateral resistant capacity.

Most of the investigations reported in the literature (Casanova *et al.* 1998, Ellis 1998, Fang *et al.* 1998) were on buildings located in high seismic zone or in countries where the windstorm is strong. In a place like Singapore, which is closer to the equator, there are no strong winds or cyclones. Furthermore, there are no seismic faults in close distance. As such the wind-induced response of the buildings could be unique due to the type of construction, and thus warrant a field investigation to assess the actual properties and the behavior of such buildings. This paper investigates this aspect as described below.

2. Field instrumentation and monitoring procedure

In order to obtain a suitable empirical forecast model for frequencies of typical buildings in Singapore, the following buildings were chosen: Marine Parade Blk14; Toa Payoh Central Blk179; Toa Payoh Lorong 8 Blk227; and Toa Payoh Central Blk155. The instrumentation used for field measurement is described with respect to the 25-story residential Blk179 in Toa Payoh Central (Fig. 1). The immediate surrounding consists of buildings of various heights ranging from 3-story shop houses to 30-story apartments.

Fig. 1 Elevation of the Blk179

2.1. Instrumentation

Two accelerometers were placed orthogonal to each other at the corner of the roof, as shown in Fig. 2(a); and an ultrasonic anemometer is also erected atop a 9 m mast on the water tank cum lift

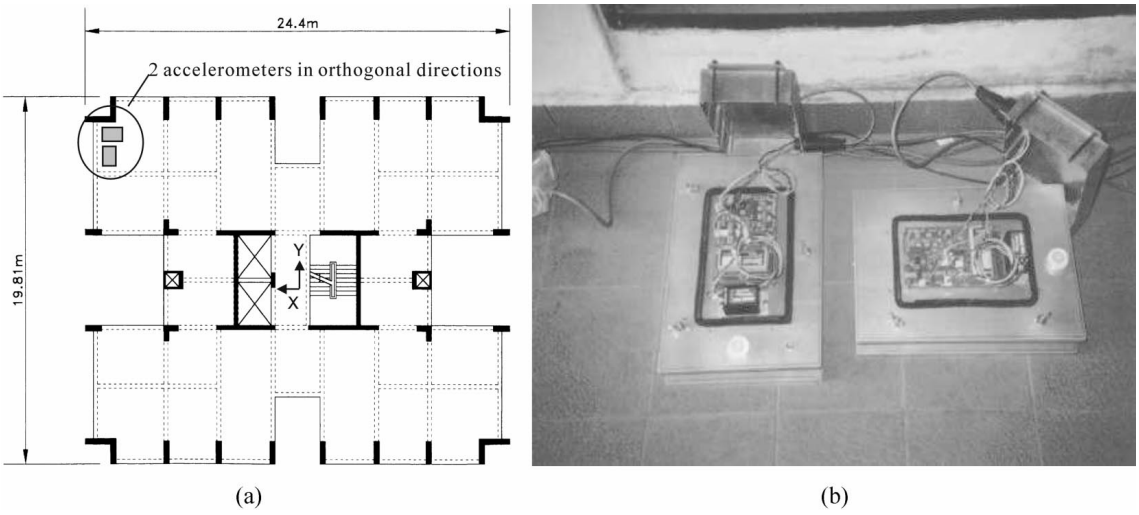

Fig. 2 (a) Plan view of the Blk179 (b) Servo accelerometers

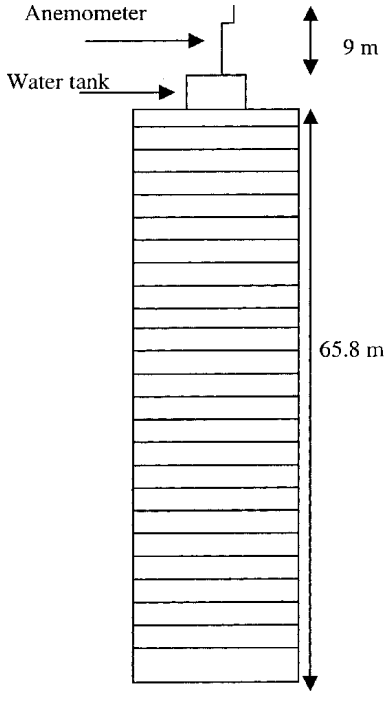

Fig. 3 Position of the anemometer

machine, as shown in Fig. 3, so as to capture the wind speed and its corresponding direction that cause the building's motion. The reason for securing the anemometer above a 9 m mast is to ensure that only ambient wind speed and direction are recorded. Disturbed wind as a result of vortex generation by the roof edges is thus eliminated or minimized. The accelerometers were subsequently shifted to the center of the buildings in order to measure the along and across wind accelerations.

2.1.1. Accelerometers

Two JEWELL servo accelerometers (Fig. 2(b)) capable of measuring acceleration up to +/−0.5G are used with a low pass filter at 10 Hz (Lyons 1997), with a signal to noise gain ratio of 50. The analogue voltage of 10V corresponding to 1G acceleration is preset via calibration set-up. The Servo accelerometer contains an electrostatics actuator that continuously acts on the seismic mass in such a way as to oppose its motion. Therefore, instead of measuring the seismic mass deflection caused by the acceleration, the motion is nulled by the proportional restoring force generated by the actuator which essentially works as an electrically controlled spring. In order to make the accelerometers endurable for the outdoor exposure, special watertight cases are designed to enclose all the sensitive electronic sensors. The seismic mass within the accelerometer has to be horizontal in order to eliminate undesirable DC signal offset.

2.1.2. Ultrasonic anemometer

The Thies Clima ultrasonic anemometer shown in Fig. 4 is used to measure the wind speeds and wind directions. It comprises two pairs of ultrasonic transformers that act as both acoustic sound transmitters and receivers. When the transformers propagate sound to each other simultaneously in the north-south and east-west directions, two perpendicular measurement paths are formed. These measurements paths are the basis from which the anemometer computes the wind speed and wind

Fig. 4 Ultrasonic anemometer

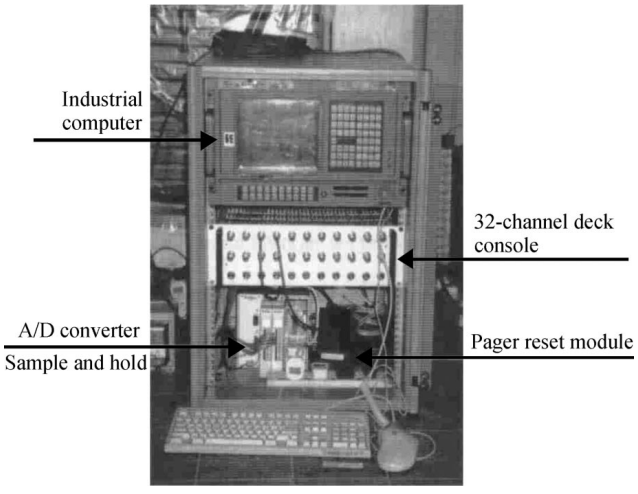

Fig. 5 Data logger

direction. During operation, the speed of sound propagation between the transformers increases when the wind speed component is in line with the direction of the sound transmission path. By combining the two measuring paths, the magnitude and angle of the wind velocity vector are obtained. The analogue voltage conversion scale factors for the wind speed and wind direction are 1V to 6 m/s and 1V to 36^o respectively, it is capable of measuring wind speed up to 60 m/s in any direction from 0^o to 360^o.

2.1.3. Data logger

The data logger system essentially consists of an industrial computer, a 32-channel deck console, an analogue to digital (A/D) converter, and a modem facility, as shown in Fig. 5. The data from the accelerometers and anemometer are collected for several hours at a sampling rate of 30 Hz. As it will take 10-minutes plus 5-minutes idle time to record one file, there will be 4 files per hour, and 96 files per day. With this setting, each channel (there are four channels) will generate $30\times60\times10$ points for one column of the data file. All data files collected in this manner, day and night, are zipped and subsequently downloaded to the laboratory via modem every week for post processing.

3. Field test results

3.1. Frequencies

To determine which file recorded the strongest vibration motion, standard deviation tests were conducted on the 10000 files collected. The top 100 files corresponding to the strongest signals were chosen for spectral analysis with 16384 points per channel for Fast Fourier Transform. This analysis transforms the acceleration time history records to a frequency domain representation from which the dominant modal frequencies are determined through the identification of resonance peaks (Clough and Penzien 1993).

Fig. 6 illustrates the power spectra curves obtained through averaging the FFT analysis of the 100 data files. It is evident that 0.836 Hz and 3.056 Hz are the resonant frequencies for translation in *X* direction, as there are no similar peaks on the spectrum derived from the data obtained from the accelerometer in *Y* direction. Similarly, 0.943 Hz and 3.35 Hz are the resonant frequencies corresponding to translation in the *Y* direction. Resonant peak picked by both accelerometers in *X* & *Y* directions at 1.073 Hz indicates that there is a torsional mode at this frequency. Based on this principle, the frequencies obtained for buildings under investigation are tabulated in Table 1.

Table 1 Field data on frequencies of residential buildings

Building	Height (m)	1st Translational Frequency (Hz)	2nd Translational Frequency (Hz)	1st Torsional Frequency (Hz)
Block 179	65.8	0.84	0.94	1.07
Block 14	66.0	0.78	0.80	0.83
Block 155	84.8	0.68	0.74	0.86
Block 227	42.0	0.99	--	1.16

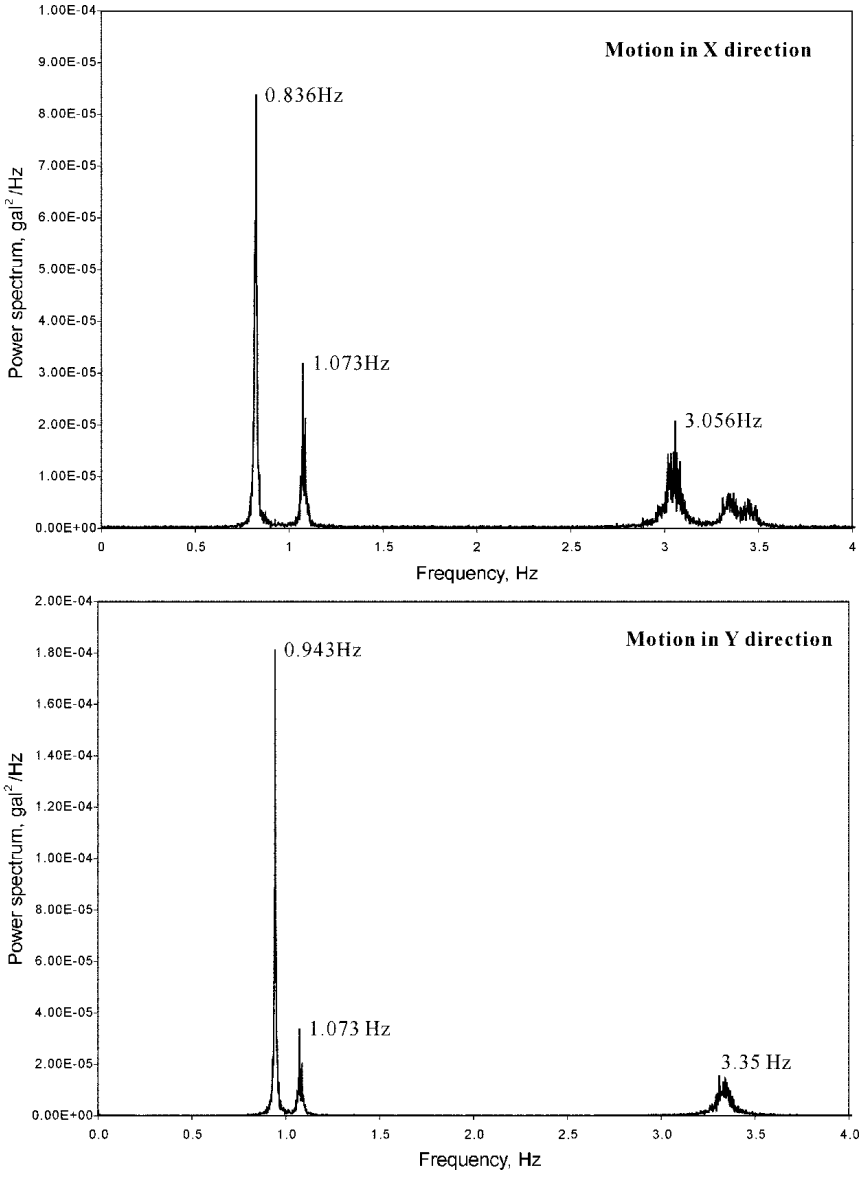

Fig. 6 Spectra of the wind- induced response in *X* and *Y* directions

3.2. Damping ratio

Estimation of the structural damping ratio, ξ, from the ambient vibration measurements can be obtained through various means such as random decrement technique (Fang *et al.* 1998), maximum likelihood technique (Casanova *et al*. 1998) and the half power band width method (Clough and Penzien 1993). In this case, the latter method has been chosen as ξ can be easily derived from the power spectrum plots obtained earlier.

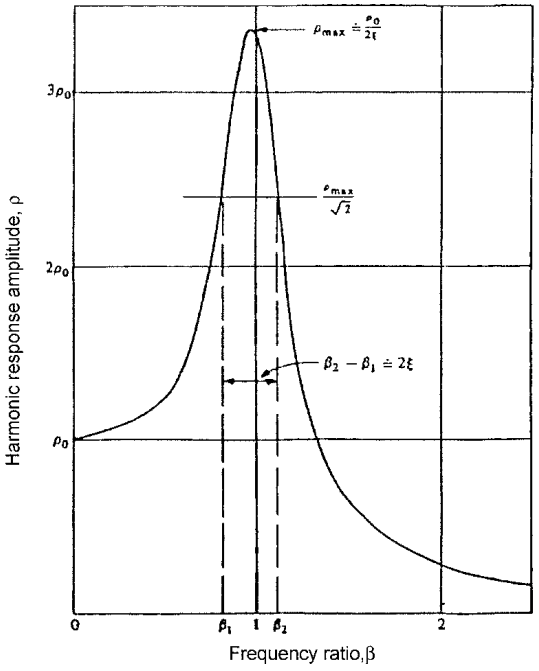

Fig. 7 Frequency response curve

Table 2 Field data on damping ratio of residential buildings

Building	Height (m)	1st Translational Damping Ratio	2nd Translational Damping Ratio	1st Torsional Damping Ratio
Block 179	65.8	0.78%	0.79%	1.01%
Block 14	66.0	1.32%	1.22%	2.00%
Block 155	84.8	1.02%	1.78%	1.81%
Block 227	42.0	1.87%	--	2.25%

To determine damping ratio, ξ, via the half power bandwidth method as shown in Fig. 7, the following equations are used:

$$\xi = \frac{\beta_2 - \beta_1}{2} \tag{1}$$

$$\beta = \frac{\omega_f}{\omega_s} \tag{2}$$

where ω_s is the frequency in Hz, corresponding to the mode shape whose damping is to be calculated and ω_f is the excitation frequency in Hz. For the instrumented buildings, results of the estimated ξ values are tabulated in Table 2.

3.3. Empirical forecast model for fundamental translational period

The choice of an appropriate structural system during the design of tall buildings depends largely

Table 3 Comparison between various empirical forecast models and field data

Empirical Forecast Model (EFM)	Expression	Blk179 (H = 65.8 m)		Blk14 (H = 66.0 m)		Blk155 (H = 84.8 m)		Blk227 (H = 42.0 m)	
		EFM T(s)	$\frac{EFM}{Field}$	EFM T(s)	$\frac{EFM}{Field}$	EFM T(s)	$\frac{EFM}{Field}$	EFM T(s)	$\frac{EFM}{Field}$
UBC (1997)	$T = 0.0731H^{0.75}$	1.69	1.41	1.69	1.32	2.04	1.38	1.21	1.19
Ellis (1998)	$T = H/46$	1.43	1.20	1.43	1.12	1.84	1.24	0.91	0.89
Lagomarsino(1998)	$T = H/55$	1.20	1.01	1.20	0.94	1.54	1.04	0.76	0.75
Ono *et al.* (1998)	$T = 0.0149H$	0.98	0.82	0.98	0.76	1.26	0.85	0.63	0.62
Hong&Hwang(2000)	$T = H/77$	0.85	0.71	0.86	0.67	1.10	0.74	0.55	0.54

Table 4 Field data (Brownjohn 2001) on frequencies of office towers

Building	Height (m)	1st Translational Frequency (Hz)	2nd Translational Frequency (Hz)
Office Tower	141	0.33	0.51
Office Tower	150	0.35	0.39
Office Tower	183	0.31	0.44
Office Tower	116	0.61	0.64

on how accurate is the assessment of the buildings' response towards lateral forces. Thus, the estimation of the fundamental vibration period which is inverse of the frequency is important. The empirical formulae available in the literature (UBC 1997, Hong and Hwang 2000, Lagomarsino 1998, Ono *et al.* 1998) are based on field measurements on buildings conducted in countries other than Singapore. Since the type of construction, structural form and design loads differ from country to country, it is important to assess which of the empirical model is suitable and even to propose an appropriate model.

Table 3 compares the ratio between the fundamental period of the buildings from various empirical models and field measurements. The ratio varies from 0.54 to 1.41, and it is evident that Lagomarsino (1998) gives the best estimate for fundamental mode, with maximum deviation of 6% for taller buildings, and 25% deviation for mid-rise buildings. Thus, in the interest of proposing a more accurate empirical formula for typical reinforced-concrete buildings in Singapore, the data in Table 1 is complemented with additional data (Brownjohn 2001) given in Table 4. From the best-fit lines as depicted in Fig. 8, the following empirical relationships for fundamental period in the weaker and stronger axes are obtained:

$$T = H/53; \quad \text{for weaker axis}$$
$$T = H/68; \quad \text{for stronger axis}$$

3.4. Empirical forecast model for fundamental torsional period

Among the literature surveyed, only Ellis (1998) and Lagomarsino (1998) are known to have provisions for estimating the fundamental torsional period. By comparing their predicted values with

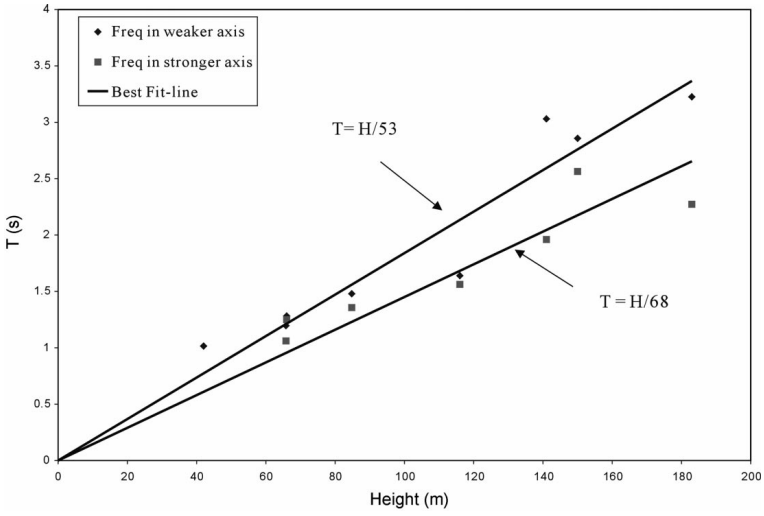

Fig. 8 The best fit-line for fundamental period

the field results as shown in Table 5, it is seen that the ratio between the empirical and field data varies from 0.63 to 1.01, and Ellis (1998) gives a slightly better estimate for fundamental torsional period with maximum deviation of 33% for mid-rise buildings, and 23% for taller buildings.

3.5. The relationship between 10-minute mean and 3-second gust speed

For the typical residential point block 179, continuous field measurements are carried out in order to obtain a relationship between RMS acceleration and wind speed for the local wind climate. Among the data files collected, only those with wind striking approximately normal to building's surface ($\beta = 0^o$ and $\beta = 90^o$) are considered. The selected files are categorized according to wind speeds before the corresponding accelerations of the building are extracted. The wind angle of incidence is defined as shown in Fig. 9.

Since each selected file contains the 10-minute recorded data, the 10-minute mean wind speed is easily calculated by averaging all the wind speed data points within the file. The 3-second gust speed is the maximum speed of all the 3-second mean wind speed within the 10-minute data file. Throughout the six months field measurements, there are 10500 files collected, only 5% of files contain the data of wind which strike at an angle normal to the building surface. Generally, the wind speed recorded is moderate. Although through January to March, there were some monsoon

Table 5 Comparison between various empirical forecast models and field data

Empirical Forecast Model (EFM)	Expression	Blk179 (H = 65.8 m)		Blk14 (H = 66.0 m)		Blk155 (H = 84.8 m)		Blk227 (H = 42.0 m)	
		EFM T(s)	$\frac{EFM}{Field}$	EFM T(s)	$\frac{EFM}{Field}$	EFM T(s)	$\frac{EFM}{Field}$	EFM T(s)	$\frac{EFM}{Field}$
Ellis(1998)	$T = H/72$	0.91	0.98	0.92	0.77	1.18	1.01	0.58	0.67
Lagomarsino(1998)	$T = H/78$	0.84	0.90	0.85	0.70	1.09	0.93	0.54	0.63

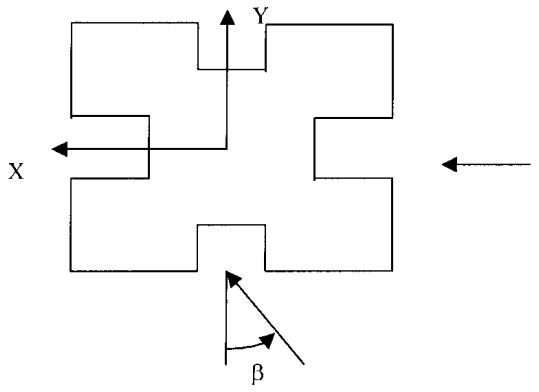

Fig. 9 Angle of incidence of wind

Table 6 Number of occurrence of different wind speed over 6 months

Wind direction \ No of occurrence		At 4-6 m/s	At 6-8 m/s	At 8-10 m/s	At 10-12 m/s	At 12-14 m/s	At 14-17 m/s
$\beta = 0^o$	10-minute mean	100	80	6	--	--	--
	3-seoncd gust	100	100	80	80	6	--
$\beta = 90^o$	10-minute mean	100	80	20	8	--	--
	3-seoncd gust	100	100	100	80	20	8

wind, the maximum recorded 10-minunte mean wind speed was about 11 m/s which occurred at the wind angle of incidence $\beta = 90^o$. The maximum 3-second gust speed was about 17 m/s which occurred at the same particular 10-minute mean wind speed file. Generally, it is found that during the field measurement period the wind that strikes at angle of incidence $\beta = 90^o$ is stronger than that strikes at angle of incidence $\beta = 0^o$. Even the number of occurrence is found to be more for $\beta = 90^o$. A statistical breakdown of the wind data obtained is summarized in Table 6.

The velocity ratio between 3-second gust speed and 10-minute mean wind speed can be calculated by the following empirical formula proposed by Deaves and Harries (AS 1170.2, 1989):

$$\text{for terrain category 2 (open terrain):} \quad \overline{U}_Z = \overline{U}_0\left(\frac{z}{300}\right)^{0.15}; \tag{3}$$

$$\text{for terrain category 4 (urban terrain):} \quad \overline{U}_Z = \overline{U}_0\left(\frac{z}{450}\right)^{0.29}; \tag{4}$$

where $\overline{U}_Z$ is the 10-minute mean wind speed at height z
$\overline{U}_0$ is the gradient speed

Thus, $\overline{U}_{10m,\,cat2} = \overline{U}_0 \times \left(\frac{10}{300}\right)^{0.15} = 0.601\overline{U}_0$ m/s;

$\overline{U}_{65.8m,\,cat4} = \overline{U}_0 \times \left(\frac{65.8}{450}\right)^{0.29} = 0.570\overline{U}_0$ m/s

According to table provided in Deaves & Harris, AS1170.2 (1989):

$$\frac{\overline{U}_{10m,\,cat2}}{\hat{U}_{10m,\,cat2}} = 0.596, \text{ thus } \hat{U}_{10m,\,cat2} = \overline{U}_{10m,\,cat2}/0.596 = 1.01\overline{U}_0 \text{ m/s};$$

where $\hat{U}_{10m,\,cat2}$ is the 3-second gust speed at the height of 10 m in terrain category 2;

$$\frac{\hat{U}_{65.8m,\,cat4}}{\hat{U}_{10m,\,cat2}} = 0.941, \text{ thus } \hat{U}_{65.8m,\,cat4} = 0.941\hat{U}_{10m,\,cat2} = 0.947\overline{U}_0 \text{ m/s};$$

where $\hat{U}_{65.8m,\,cat4}$ is the 3-second gust speed at the height of 65.8 m in terrain category 4;

So the ratio between the 3-second gust speed and the 10-minute mean wind speed at the top of the building (+65.8 m) is $\frac{\hat{U}_{65.8m,\,cat4}}{\overline{U}_{65.8m,\,cat4}} = \frac{0.947\overline{U}_0}{0.570\overline{U}_0} = 1.661$, which is comparable with the ratio 1.667 calculated from the field test data (Table 7).

Table 7 Relationship between 10-minute mean and 3-second gust speed

10-min mean wind speed (m/s) (a)	3-second gust speed (m/s) (b)	Ratio (b)/(a)
5.090	8.502	1.670
5.112	8.906	1.735
5.396	8.790	1.629
5.538	9.251	1.670
5.576	9.762	1.751
5.598	9.627	1.719
5.623	9.303	1.654
5.716	9.953	1.737
5.778	9.638	1.668
5.911	10.196	1.709
5.916	9.688	1.638
5.925	9.958	1.679
5.993	10.107	1.680
6.027	10.243	1.692
6.091	10.112	1.660
6.123	10.087	1.637
6.221	10.540	1.694
6.333	10.437	1.648
6.338	11.075	1.736
6.854	10.736	1.566
7.299	11.031	1.511
8.305	14.000	1.686
8.652	14.800	1.711
9.621	15.900	1.653
9.836	16.325	1.659
9.956	16.447	1.652
10.156	16.493	1.624
10.232	16.300	1.593
11.030	17.300	1.568
	Total average	= **1.667**

3.6. Turbulence spectra

The simulation of natural wind in urban terrain was carried out by Balendra *et al*. (2002) in NUS-HDB wind tunnel. During the experiment, the measured turbulence spectra in the wind tunnel are compared well with the Von Karman spectrum (Scanlan and Simiu 1996). In order to have a further understanding of turbulence spectra, the field turbulence spectra are computed and compared with Von Karman spectrum (Scanlan and Simiu 1996).

Figs. 10(a) & (b) show the comparison between the field turbulence spectra and Von Karman spectrum for $\beta = 0^o$ and $\beta = 90^o$ respectively. It is seen that the measured turbulence spectra are comparing well with the Von Karman spectrum. For $\beta = 0^o$, the longitudinal integral length scale, which defines the size of eddies is determined using the expression, $L_u^x = \overline{U}/2\pi n' = 151$ m, in which n' is the frequency corresponding to the spectral peak as obtained from the plotted values of normalized spectrum, $nS_u(n)/\sigma_u^2$. For $\beta = 90^o$, the corresponding longitudinal integral length scale, $L_u^x = \overline{U}/2\pi n'$, is 149 m.

3.7. RMS acceleration

Figs. 11(a)&(b) show the RMS accelerations in along wind and across wind directions respectively for wind angle of incidence $\beta = 90^o$. For comparison, the empirical estimation results from AIJ (1996) and Vickery (Vickery 1973, see Appendix) and Australian Code (Australian/New Zealand Standard 2000) are presented.

It is seen from Fig. 11(b) that the field data for across wind acceleration compare well with AIJ and Vickery for wind speeds greater than 5 m/s. The AIJ (1996) seems to slightly underestimate the along wind response (Fig. 11(a)). However, the Australian Code (in terms of 3-second gust speed, see appendix) compares well with the measured along wind acceleration as depicted in Fig. 11(c). The across wind accelerations in the Australian Code are given for much higher wind speed than what was encountered in Singapore, as such, the comparison was not made for across wind motions.

For $\beta = 0^o$, the maximum 10-minute mean and 3-second gust wind speed recorded are 8.9 m/s and

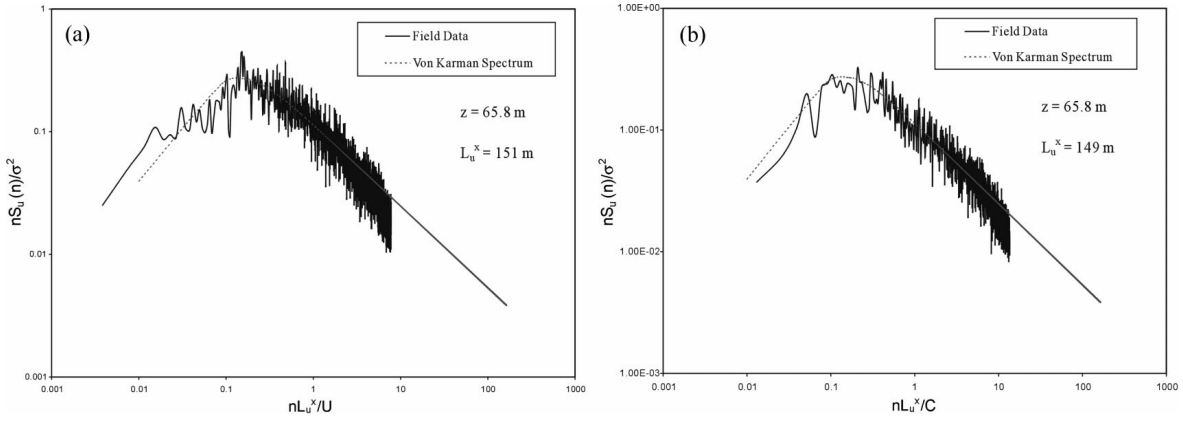

Fig. 10 (a) Field velocity spectrum for $\beta = 0^o$, (b) Field velocity spectrum for $\beta = 90^o$

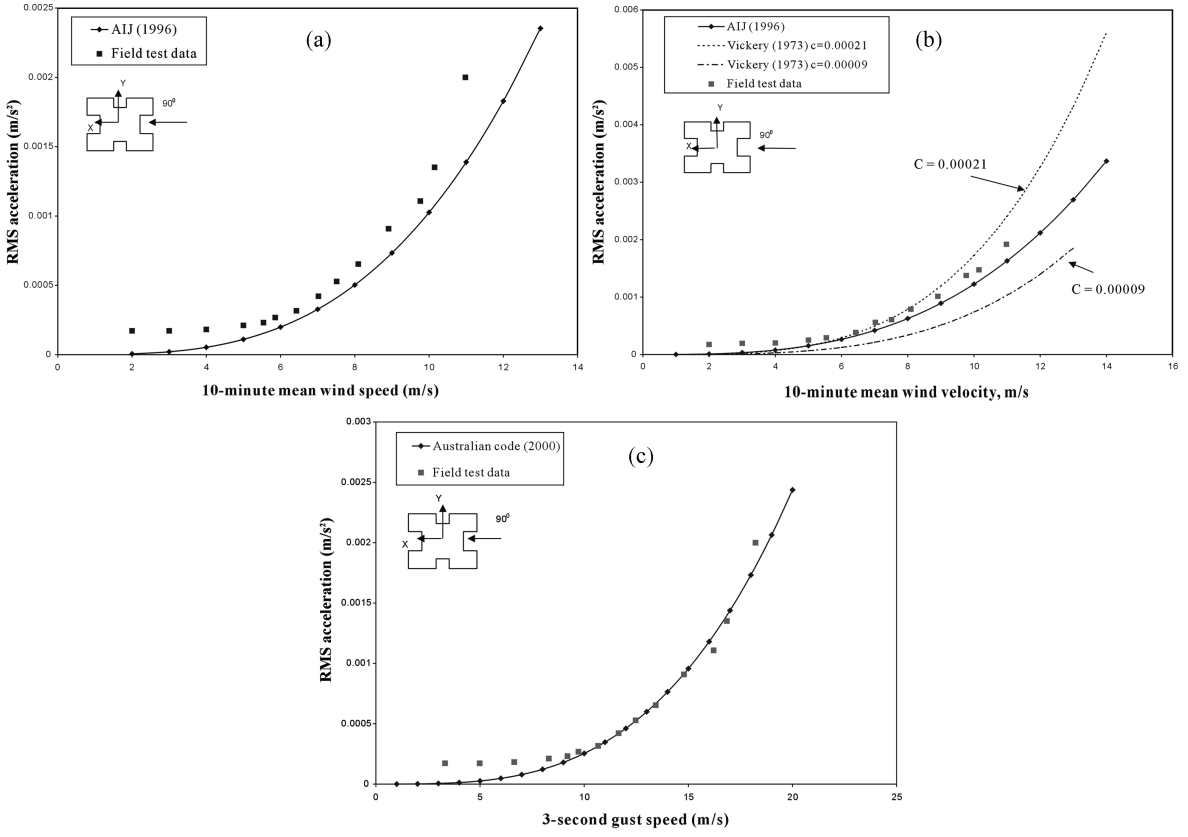

Fig. 11 (a) Along wind RMS acceleration at $\beta = 90^o$, (b) Across wind RMS acceleration at $\beta = 90^o$, (c) Along wind RMS acceleration at $\beta = 90^o$

14.7 m/s respectively. Figs. 12(a)&(b) show the RMS accelerations in along wind and across wind direction respectively for 10-minute mean wind speed, and comparison with AIJ and Vickery. Fig. 12(c) shows the along wind RMS accelerations for 3-second gust speed and comparison with Australian Code. It is seen from Fig. 12(a) that AIJ compares well with the field data for along wind acceleration. Any deviation observed is because of lack of sufficient number of occurrences of high wind speed. With regard to across wind acceleration, as seen from Fig. 12(b) that AIJ slightly underestimates the RMS acceleration. However, the field data for across wind acceleration compares well with Vickery. The Australian Code (in terms of 3-second gust speed) compares well with measured along wind accelerations as depicted in Fig. 12(c).

4. Numerical analysis of frequencies of vibration

In order to validate the commonly adopted computer model with the field data, computer program ETABS (1997) was used. Similar to most approaches, the buildings were first modeled as a bare frame considering only the structural elements such as beams, columns and shear walls for the overall stiffness. The ETABS results are tabulated in Table 8. When compared with Table 1, ETABS

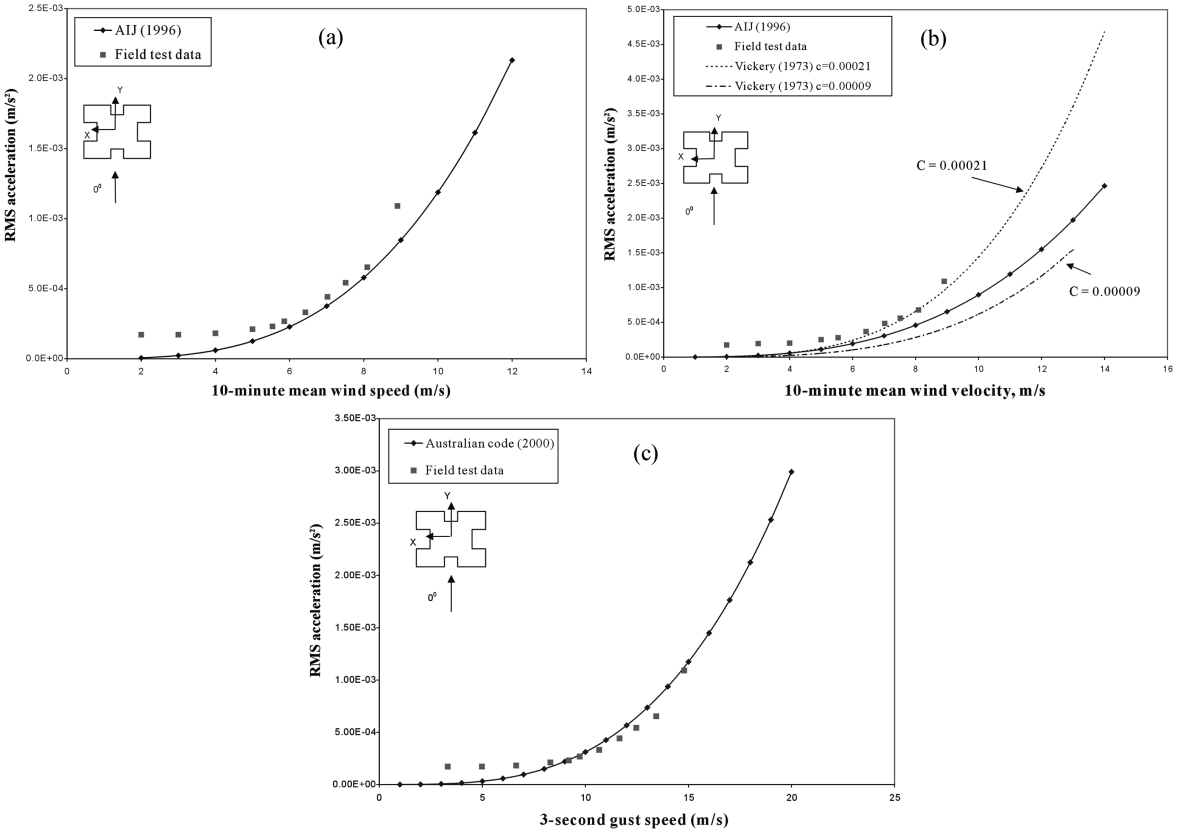

Fig. 12 (a) Along wind RMS acceleration at $\beta = 0^o$, (b) Across wind RMS acceleration at $\beta = 0^o$, (c) Along wind RMS acceleration at $\beta = 0^o$

Table 8 Comparison of ETABS results between bare frame and braced frame

*N*th frequency mode	Bare frame model				Braced frame model			
	Blk179	Blk14	Blk227	Blk155	Blk179	Blk14	Blk227	Blk155
1st *X* translation	0.42	0.37	0.78	0.34	0.78	0.78	1.18	0.61
1st *Y* translation	0.44	0.39	1.12	0.43	0.98	0.84	1.44	0.66
1st torsion	0.49	0.47	1.35	0.46	1.11	1.04	1.75	0.76

analysis gives much lower frequencies; underestimates by nearly 50% as depicted in Table 9.

The possible reason for this is due to the role of the infill walls. Under the lateral load, infill walls act as compressive diagonal members due to confinement between the walls and structural frames (Fig. 13). As a result, the overall lateral rigidity of the building is increased tremendously (Balendra *et al.* 1999). Thus, the computer model is refined by representing the non-structural full height wall by an equivalent compressive diagonal strut whose effective area, A_i, is calculated based on the following relation (Mainstone 1974).

Table 9 Comparison of analytical and field results

*N*th frequency mode	ETABS analysis with bare frame model				ETABS analysis with braced frame model			
	Analytical / Field				Analytical / Field			
	Blk179	Blk14	Blk227	Blk155	Blk179	Blk14	Blk227	Blk155
1st *X* translation	0.50	0.47	0.79	0.50	0.93	1.00	1.19	0.91
1st *Y* translation	0.47	0.49	--	0.58	1.04	1.05	--	0.90
1st torsion	0.46	0.57	1.16	0.54	1.03	1.25	1.50	0.89

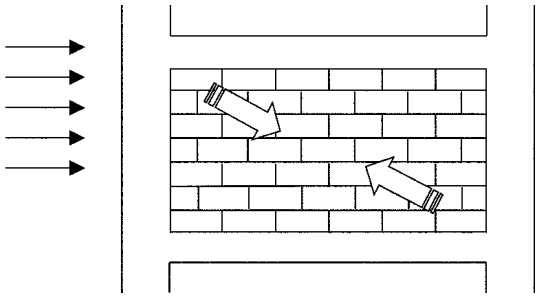

Fig. 13 Compressive diagonal forces on brick wall due to lateral load

$$A_i = w_e t \tag{5}$$

$$w_e = 0.175\ (\lambda h)^{-0.4}\, w' \tag{6}$$

$$\lambda = \sqrt[4]{\frac{E_i t \sin(2\theta)}{4 E_f I_c h'}} \tag{7}$$

where A_i is the effective strut area in in^2; E_i the modulus of elasticity of the infill material in ksi; E_f the modulus of elasticity of the frame material in ksi; I_c the moment of inertia of column in in^4 and t the thickness of infill in inches. The symbols for h, h', w' and θ are indicated in Fig. 14.

The refined model for the 25-story building Blk179 is presented in Fig. 15. Two diagonal struts are used to simulate the infill walls, both interior and exterior. The properties of each strut are calculated using Eqs. (5)-(7). Results of the ETABS analysis for this braced frame model are tabulated in Table 8, and compared with the field data in Table 9. It is seen that the braced frame model produces translational frequencies within 10% of the field data for taller buildings and within 20% for mid-rise buildings. For torsional frequencies, there is a significant improvement with a maximum difference of 25% instead of 54% for taller buildings.

This analysis clearly signals the significant contribution from infill brick walls and partition walls to the overall rigidity of the building towards wind-induced responses, which are low amplitude motions and during which the integrity of walls are intact. Had the bare frame results been used for design, the building would have been conceived as much slender and flexible with a longer period of vibration under lateral forces. Consequently, bigger size structural components would be chosen

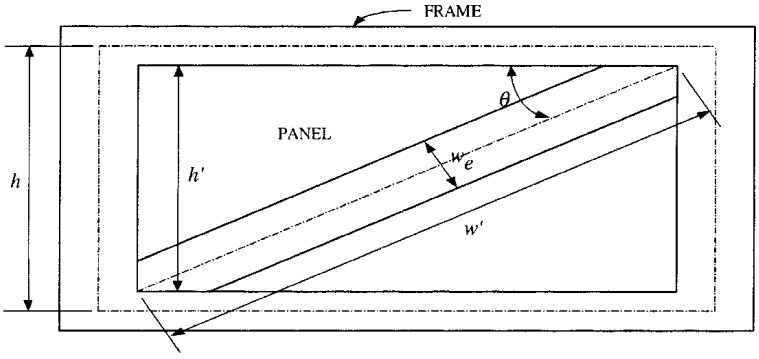

Fig. 14 Dimensions of an idealized infill frame as a frame-diagonal strut system

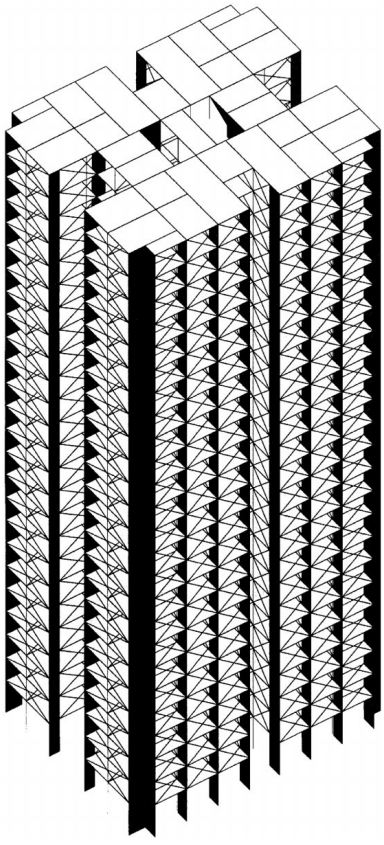

Fig. 15 3-D ETABS model

to reduce the excessive drift calculated. Hence, the merits for proper modeling points towards more cost effective and economical design for serviceability. On the other hand, a stiffer building would attract higher forces and inaccurate assessment of the building's stiffness could lead to the under-estimation of forces in the structural elements.

5. High-frequency force balance test

In order to complement the results with the full-scale field measurements, force balance test with surrounding buildings was conducted in a wind tunnel which has a working section of 2.85 m wide, 19 m long and an adjustable roof that provides section height varying from 1.8 m to 2.3 m. A balsa wood model of the prototype building, block 179, was built with length ratio of 1:375. The surrounding buildings within 0.5 km radius from block 179 were also built under the same length ratio (Fig. 16). Under the urban terrain wind simulation, the wind tunnel test was conducted using a force balance sensor JR3 (67M25-ISO40-15LB).

5.1. Principles of force balance

The fundamental principle of the force balance technique is that the modal forces due to wind loads can be estimated from the measured base moments experienced by a rigid model. This principle stands as tall buildings have a fundamental mode shape which is approximately a straight line. The rigid model is mounted on a highly sensitive and stiff force balance sensor that measures the base overturning and torsional moments (Obasaju 1992).

The governing equation of motion of the structure is expressed as

$$M(z)\ddot{x}(z,t) + C(z)\dot{x}(z,t) + K(z)x(z,t) = F(z,t) \tag{8}$$

where $M(z)$, $C(z)$ and $K(z)$ are the mass, damping coefficient, stiffness per unit height of the system respectively. If the displacement, $x(t)$ can be expressed in modal coordinate $q(t)$ as $x(z,t) = \phi(z)q(t)$, where $\phi(z)$ is the mode shape. Then, Eq. (8) can be written as

$$M_r^*\ddot{q}_r + C_r^*\dot{q}_r + K_r^* q_r = F_r^*(t) \qquad r = 1, 2, \ldots, n. \tag{9}$$

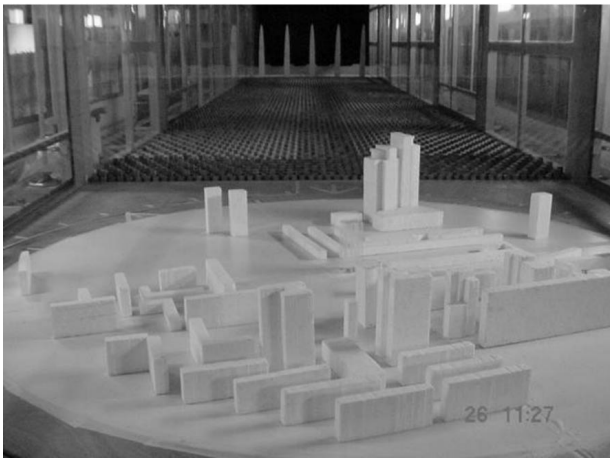

Fig. 16 Immediate surrounding buildings within 0.5 km radius from Blk 179 model in simulated boundary layer

Since the mode of vibration is assumed to be linear, $\phi_1=z/H$, for constant mass per unit height, m_0, while for the first fundamental mode shape:

$$M_1^* = \int_0^H m_0\phi_1^2 dz = \int_0^H m_0\left(\frac{z}{H}\right)^2 dz$$
$$= \frac{1}{3}m_0 H \tag{10}$$

$$K_1^* = w_1^2 M_1^*$$
$$= (2\pi n_1)^2 M_1^* \tag{11}$$

In which m_0 is mass per unit height and n_1 is fundamental sway frequency of the building. $F_1^*(t)$ can be obtained from the measured base overturning moments, $M(t)$ using the following relationship:

$$F_1^*(t) = \int_0^H F(t)\phi_1(z)dz = \frac{1}{H}\int_0^H F(t)z\,dz$$
$$= \frac{M(t)}{H} \tag{12}$$

Where H is the total building's height.

Using the random vibration theory, the power spectrum of the response can be expressed as

$$S_x = \phi_1^2(z)\frac{1}{K_1^{*2}}|H_1(n)|^2 S_{F_1^*}(n) \tag{13}$$

where $S_{F_1^*}$ is generalized wind force spectrum which is equivalent to measured moment spectrum divided by the square of the building's height. Or in other words, the power spectrum of the measured base moment S_M is proportional to the power spectrum of the generalized force $S_{F_1^*}$ for a linear mode. Since the base overturning moment generated by F_x is denoted by M_y, and that generated by F_y is denoted by M_x, thus:

$$S_{F_1^* x} = \frac{S_{My}}{H^2} \quad \text{and} \quad S_{F_1^* y} = \frac{S_{Mx}}{H^2} \tag{14}$$

and $|H_1(n)|$ is the mechanical admittance function expressed as

$$|H_1(n)| = \frac{1}{\left(\left[1-\left(\frac{n}{n_1}\right)^2\right]^2 + 4\varsigma_1^2\left(\frac{n}{n_1}\right)^2\right)^{1/2}} \tag{15}$$

The variance or mean square value of the displacement is obtained from

$$\sigma_x^2 = \int_0^\infty S_x(n)dn$$
$$= \left(\frac{z}{H}\right)^2 \frac{1}{K_1^{*2}} \int_0^\infty |H_1(n)|^2 S_{F_1^*}(n)dn \tag{16}$$

Since the linear mode shape is assumed, only the tip displacement is required to be computed from the power spectral density of modal force. Therefore the variance of tip displacement can be taken as

$$\sigma_x^2 = \frac{1}{K_1^{*2}} \int_0^\infty |H_1(n)|^2 S_{F_1^*}(n)dn$$
$$= \frac{1}{K_1^{*2}} \int_0^{n_1 - \Delta n} S_{F_1^*}(n)dn + \frac{\pi n_1 S_{F_1^*}(n)}{4\varsigma_1 K_1^{*2}}$$
$$= \frac{\sigma_{F_1^*}^2}{K_1^{*2}} + \frac{\pi n_1 S_{F_1^*}(n)}{4\varsigma_1 K_1^{*2}} \tag{17}$$

while RMS acceleration $\ddot{\sigma}_x$ as

$$\ddot{\sigma}_x = (2\pi n_1)^2 \sigma_x \tag{18}$$

Once the tip RMS acceleration $\ddot{\sigma}_D$ is found, the wind-induced forces can be calculated from the base overturning moment power spectra measured from the force balance test. The peak values of the wind-induced loads in *X* and *Y* directions are obtained from (Balendra 1993):

$$F_{x,\max}(z) = \overline{F}_x(z) + [(g_B \sigma_{B,Fx}(z))^2 + (g_{Dx} \sigma_{D,Fx}(z))^2]^{1/2} \tag{19}$$

$$F_{y,\max}(z) = \overline{F}_y(z) + [(g_B \sigma_{B,Fy}(z))^2 + (g_{Dy} \sigma_{D,Fy}(z))^2]^{1/2} \tag{20}$$

where $\overline{F}(z)$ is the mean component of the wind load;
g_B is the peak factor of background component, taken as 3.5
$\sigma_{B,F}$ is the non-resonating component or background force
$g_D = \sqrt{2\ln(600n_1)}$, the resonant peak factor, n_1 is the fundamental frequency
$\sigma_{D,F}$ is the resonating component or inertia force

The mean, non-resonant and resonant forces along the building height are calculated from the Eqs. (21)-(44) as follows:

5.1.1. For resonant force:

Since the mode of vibration is linear, the acceleration along *x*-axis and *y*-axis at any height *z* will be

$$\ddot{\sigma}_{Dx}(z) = \phi \times \ddot{\sigma}_{Dx} \tag{21}$$

$$\ddot{\sigma}_{Dy}(z) = \phi \times \ddot{\sigma}_{Dy} \tag{22}$$

The inertia force $\sigma_{D,F}(z)$ is calculated by multiplying the lumped mass at a particular floor and the corresponding acceleration as follows:

$$\sigma_{D,F_x}(z) = m_0 \Delta z \ddot{\sigma}_{Dx}(z) \tag{23}$$

$$\sigma_{D,F_y}(z) = m_0 \Delta z \ddot{\sigma}_{Dy}(z) \tag{24}$$

where Δz is inter-story height, m_0 is mass per unit height.

By multiplying the computed inertial force $\sigma_{D,F}(z)$ with the corresponding peak factor g_D, the distribution of peak inertial forces along the height of the building can be determined.

5.1.2. For mean force:

Since mean wind force is proportional to the square of mean wind velocity $\overline{U}(z)$, the mean force distribution can be determined by employing a generally accepted *power law* distribution as follows:

$$\overline{F}_X(z) = P_x(z) B_X \Delta z \tag{25}$$

$$\overline{F}_y(z) = P_y(z) B_y \Delta z \tag{26}$$

where B_X, B_Y are the breadth of the building in X, Y direction, Δz is inter-story height, $P_x(z)$, $P_Y(z)$ are the mean pressure at height z in X and Y directions respectively. $P_x(z)$ and $P_Y(z)$ can be calculated from following Eqs. (27)-(38):

The mean overturning moment coefficients are defined as the mean values of measured overturning moments $\overline{M}$ normalized by $\frac{1}{2}\rho_{air}\overline{U}_H^2 BH^2$. Where ρ_{air} is the air density which is 1.2 kg/m^3, $\overline{U}_H$ is the mean wind speed at the tip of the building, B and H are the breadth and height of the building respectively. Thus the mean overturning moment coefficients about the X and Y axes are defined as:

$$C_{\overline{M}_x} = \frac{\overline{M}_x}{\frac{1}{2}\rho_{air}\overline{U}_H^2 BH^2} \tag{27}$$

$$C_{\overline{M}_y} = \frac{\overline{M}_y}{\frac{1}{2}\rho_{air}\overline{U}_H^2 BH^2} \tag{28}$$

so $\overline{M}_x$ and $\overline{M}_y$ can be related to the mean pressure distribution as

$$\begin{aligned} \overline{M}_x &= \frac{1}{2}\rho_{air} C_{\overline{M}_x} \overline{U}_H^2 BH^2 \\ &= \int_0^H B P_y(z) z \, dz \end{aligned} \tag{29}$$

$$\overline{M}_y = \frac{1}{2}\rho_{air} C_{\overline{M}_y} \overline{U}_H^2 BH^2$$
$$= \int_0^H BP_x(z) z\,dz \tag{30}$$

where $P_x(z)$ and $P_y(z)$ can be related to the mean pressure at the top of the building, P_{0x} and P_{0y} as:

$$\frac{P_y(z)}{P_{0y}} = \left(\frac{z}{H}\right)^{2\alpha} \tag{31}$$

$$\frac{P_x(z)}{P_{0x}} = \left(\frac{z}{H}\right)^{2\alpha} \tag{32}$$

where α is the power law exponential of urban terrain profile, taken as 0.29. Hence, the mean base overturning moment about the *x* and *y*-axes can be expressed as follows:

$$\overline{M}_x = P_{0y} B \int_0^H \left(\frac{z}{H}\right)^{2\alpha} z\,dz \tag{33}$$

$$\overline{M}_y = P_{0x} B \int_0^H \left(\frac{z}{H}\right)^{2\alpha} z\,dz \tag{34}$$

In view of Eqs. (31) and (32),

$$P_{0x} = (\alpha + 1)\rho_{air} C_{\overline{M}_y} \overline{U}_H^2 \tag{35}$$

$$P_{0y} = (\alpha + 1)\rho_{air} C_{\overline{M}_x} \overline{U}_H^2 \tag{36}$$

Hence the pressure at height, *z* of the building, $P_x(z)$ and $P_y(z)$ can be easily determined as

$$P_x(z) = (\alpha + 1)\rho_{air} C_{\overline{M}_y} \overline{U}_H^2 \left(\frac{z}{H}\right)^{2\alpha} \tag{37}$$

$$P_y(z) = (\alpha + 1)\rho_{air} C_{\overline{M}_x} \overline{U}_H^2 \left(\frac{z}{H}\right)^{2\alpha} \tag{38}$$

Once $P_x(z)$ and $P_y(z)$ are determined, mean forces can be calculated by applying Eqs. (25) and (26).

5.1.3. For non-resonant force:

The same definitions apply for the non-resonant or background component of wind forces with the assumption that the background wind forces follow the mean force distribution, i.e., *power law* distribution. This assumption is based on the fact that fluctuating background wind forces are formed of long period waves which can be approximated as static forces. To determine the background wind pressure, the RMS moment coefficients, $C_{\sigma_{M_x}}$ and $C_{\sigma_{M_y}}$ are employed to replace mean moment coefficients, $C_{\overline{M}_x}$ and $C_{\overline{M}_y}$.

Thus, the non-resonant force can be calculated as follows:

$$\sigma_{B,\,Fx}(z) = P_{\sigma x}(z) B_X \Delta z \tag{39}$$

$$\sigma_{B,\,Fy}(z) = P_{\sigma Y}(z) B_Y \Delta z \tag{40}$$

$$\text{where } P_{\sigma x}(z) = (\alpha + 1)\rho_{air} C_{\sigma M_X} \overline{U}_H^2 \left(\frac{z}{H}\right)^{2\alpha} \tag{41}$$

$$P_{\sigma Y}(z) = (\alpha + 1)\rho_{air} C_{\sigma M_Y} \overline{U}_H^2 \left(\frac{z}{H}\right)^{2\alpha} \tag{42}$$

$C_{\sigma M_X}$ and $C_{\sigma M_Y}$ are defined as the same manner as Eqs. (27) and (28), thus

$$C_{\sigma M_x} = \frac{\sigma_{M_x}}{\frac{1}{2}\rho_{air}\overline{U}_H^2 B H^2} \tag{43}$$

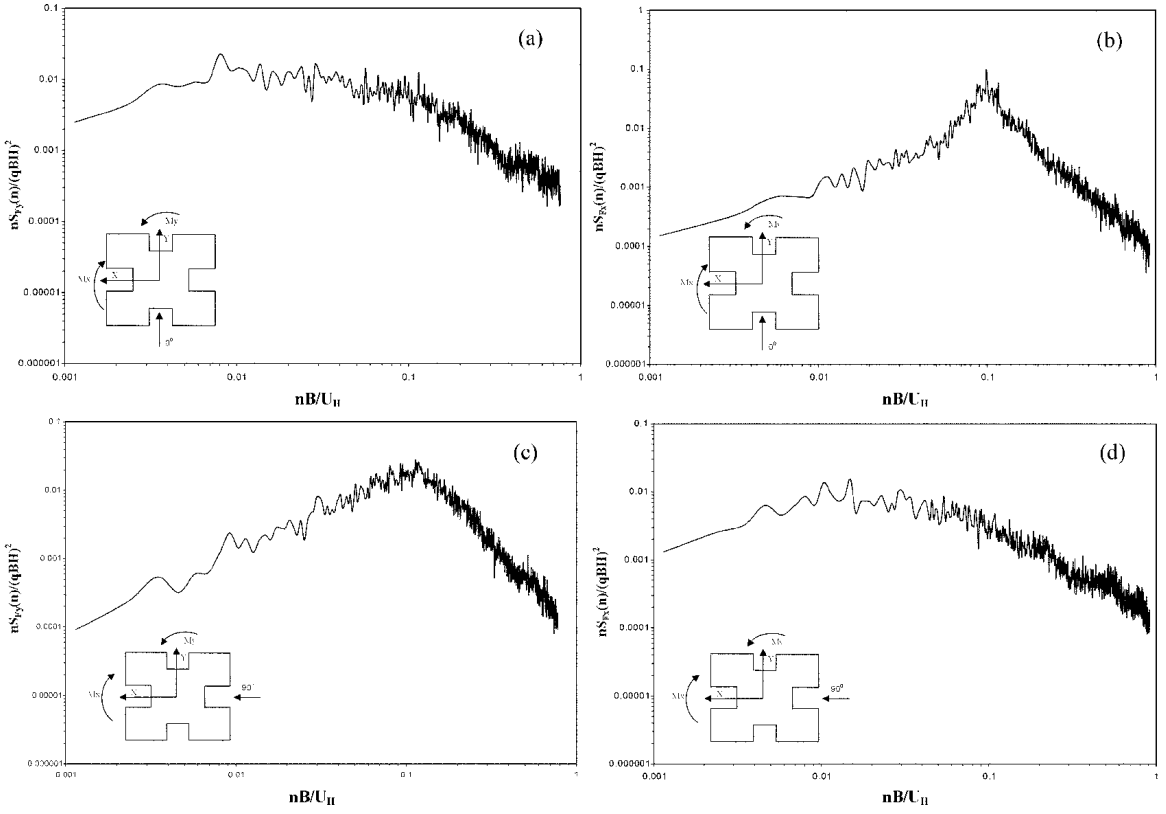

Fig. 17 (a) Modal force power spectra S_{Fy} for $\beta = 0^o$, (b) Modal force power spectra S_{Fx} for $\beta = 0^o$, (c) Modal force power spectra S_{Fy} for $\beta = 90^o$, (d) Modal force power spectra S_{Fx} for $\beta = 90^o$

$$C_{\sigma M_y} = \frac{\sigma_{M_y}}{\frac{1}{2}\rho_{air}\overline{U}_H^2 BH^2} \tag{44}$$

σ_{M_x} and σ_{M_y} are the RMS values of the measured overturning moments M_x and M_y respectively.

5.2. Modal force power spectra

The modal force power spectra can be obtained by dividing the base overturning moment power spectra by H^2 (Eq. (14)). As the maximum overturning moments about X and Y axes occur when the wind angles of incidence are about $\beta = 0^o$ and $\beta = 90^o$, only the modal force spectra in these two angles are considered. The modal force power spectra S_{Fy} and S_{Fx} for angle of incidence $\beta = 0^o$ are plotted in Figs. 17(a)&(b) respectively. Figs. 17(c)&(d) present the modal force power spectra S_{Fy} and S_{Fx} for angle of incidence $\beta = 90^o$ respectively.

The modal force spectra are presented in the form $nS_F(n)/(qBH)^2$ versus $nB/\overline{U}_H$. where n is the

Table 10 Distribution of wind total forces along Y and X-axes

Height (m)	Total force (kN) (along Y-axis, B=24.4 m) $\beta = 0^o$			Total force (kN) (along X-axis, B=19.8 m) $\beta = 90^o$		
	Wind tunnel results	Australian Code (2000)	CP3 (1972)	Wind tunnel results	Australian Code (2000)	CP3 (1972)
0.00	0.00	0.00	0.00	0.00	0.00	0.00
3.43	7.33	20.00	10.70	5.77	20.00	8.50
5.96	8.60	27.44	10.63	6.76	22.39	8.45
8.50	10.59	27.50	12.36	8.32	22.44	9.83
11.03	12.36	27.56	14.04	9.70	22.50	11.16
13.56	13.98	27.63	15.51	10.96	22.55	12.33
16.09	15.49	27.69	17.06	12.13	22.60	13.56
18.62	16.91	27.75	18.69	13.23	22.66	14.85
21.16	18.26	27.83	20.19	14.28	22.73	16.05
23.69	19.56	28.39	21.51	15.27	23.19	17.09
26.22	20.80	28.95	22.86	16.23	23.66	19.28
28.75	22.01	29.52	24.26	17.15	24.13	19.28
31.28	23.17	30.10	25.79	18.04	24.61	20.49
33.82	24.31	30.69	27.44	18.91	25.10	21.81
36.35	25.41	31.28	29.14	19.75	25.60	23.16
38.88	26.49	31.60	31.45	20.57	26.09	24.55
41.41	27.55	32.47	32.19	21.37	26.59	25.58
43.94	28.58	33.08	33.11	22.16	27.09	26.31
46.48	29.60	33.69	34.04	22.93	27.61	27.05
49.01	30.59	34.31	34.98	23.68	28.12	27.80
51.54	31.57	34.93	35.81	24.42	28.65	28.46
54.07	32.54	35.45	36.58	25.15	29.08	29.07
56.60	833.49	35.97	37.36	25.87	29.52	29.69
59.14	34.43	36.50	38.15	26.57	29.96	30.32
61.67	45.24	45.00	50.99	35.21	45.00	40.52
65.80	35.41	30.62	32.28	26.05	25.15	25.66

frequency; $S_F(n)$ is the modal force spectral density; $q = \frac{1}{2}\rho_{air}\overline{U}_H^2$; B=0.0651 m, which is the wider breadth of the model; H=0.176 m, which is the height of the model; $\overline{U}_H$ = 6.9 m/s, which is the mean velocity at the tip of the model in wind tunnel.

The across-wind spectra in Figs. 17(b)&(c) have sharp peaks at reduced frequencies (or Strouhal Number) of about 0.1 and 0.12 respectively. But the vortex peak for $\beta = 0^o$ is sharper than that for $\beta = 90^o$. This suggests that there is organized vortex shedding for $\beta = 0^o$ but not for $\beta = 90^o$. Figs 17(a)&(d) show the along-wind modal force spectra for $\beta = 0^o$ and $\beta = 90^o$ respectively. These broadband type of spectra imply that the fluctuating wind force due to along wind is random.

5.3. Wind-induced loads by force balance

For ultimate design (1 in 50 year gradient mean wind speed of 33 m/s at 450 m), the maximum wind load distribution along the height of the building is important for the design of structural components. The critical angles of wind incidence for overturning moments are those angles near 0° for moment about X-axis and 90° for moment about Y-axis. Thus it is of particular interest to compare the wind-induced loads at angles $\beta = 0^o$ and $\beta = 90^o$.

Once the modal force power spectra are obtained, the wind-induced force distribution along the building height can be calculated based on the principles (Eqs. (19)-(44)) discussed in the previous section. The along wind force distribution for angle of incidence $\beta = 0^o$ and $\beta = 90^o$ are depicted in Figs. 18(a)&(b).

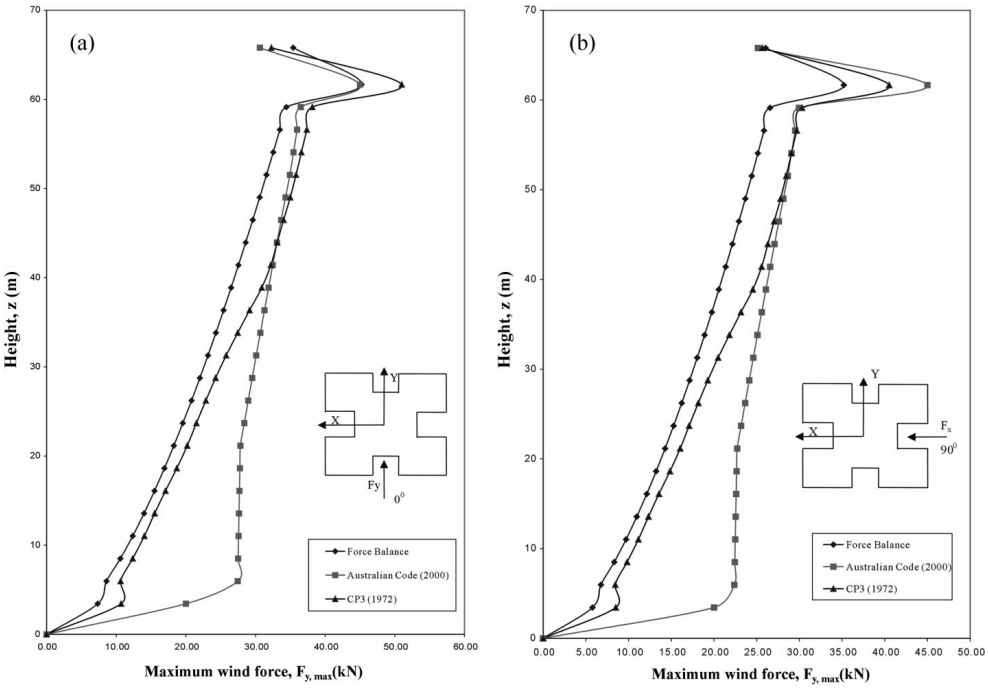

Fig. 18 (a) The comparison of total wind-induced force along Y-axis for β = 0°, (b) The comparison of total wind-induced force along X-axis for β = 90°

5.4. Comparison of wind-induced load with wind codes

The results of along wind-induced loads for $\beta = 0^o$ and $\beta = 90^o$ calculated using Australian Code (Australian/New Zealand Standard, 2000) and CP3 (Code of basic data for the design of buildings, 1972, as described in the appendix) are tabulated in Table 10, and depicted in Figs. 18(a)&(b).

For along wind-induced loads in the wind angle of incidence of $\beta = 0^o$ as shown in Fig. 18(a), the total base shear along the *Y*-axis calculated from force balance test is 595 kN, while the total base shear forces predicted by CP3 and Australian Code are 667 kN and 776 kN respectively. The CP3 over-estimates the total base shear force by 12%, while Australian Code over-estimates by 30%. It is seen from Fig. 18(a) that the CP3 tends to give a good prediction on distribution of wind loads along the height of the building, while the Australian Code overestimates the wind-induced load for the lower one-third height of the building. For the angle of incidence of $\beta = 90^o$ as shown in Fig. 18(b), the total base shear along the *X*-axis calculated from force balance test is 461 kN, while the corresponding results predicted by CP3 and Australian Code are 529 kN and 647 kN respectively. The CP3 over-estimates the total base shear force by 14%, while Australian Code over-estimates by 40%. The distribution trend is similar to $\beta = 0^o$.

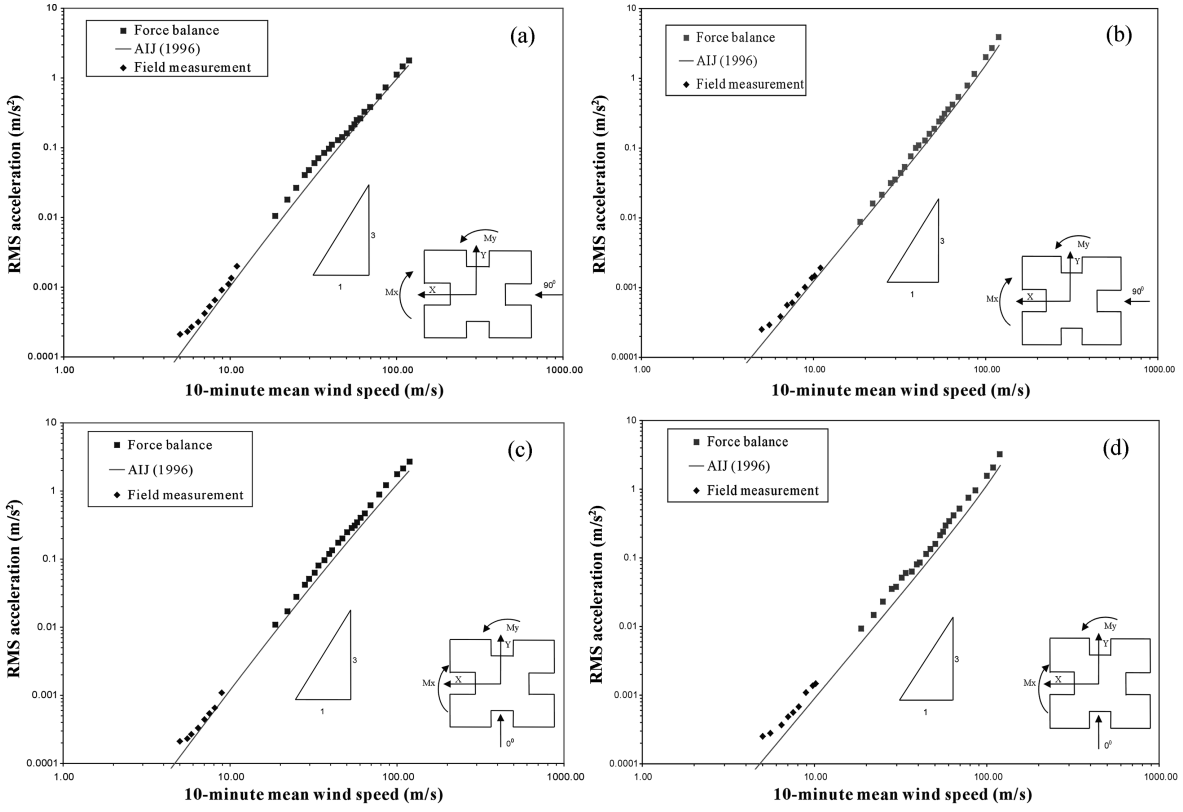

Fig. 19 (a) Along wind acceleration for $\beta = 0^o$, (b) Across wind acceleration for $\beta = 90^o$, (c) Along wind acceleration for $\beta = 0^o$, (d) Across wind acceleration for $\beta = 0^o$

5.5. RMS acceleration

Since there is lack of data on the upper range of the wind speeds, the results generated in the wind tunnel by using the force balance technique are used to complement the field test data. Both wind tunnel and field test data are compared with AIJ (1996) for along and across wind as depicted in Figs. 19(a)-(d).

It is seen that the field test and wind tunnel test results are falling in line with the AIJ prediction, for both along and across wind acceleration. The RMS accelerations from both wind tunnel test and field measurement increase in proportion to approximately the third power of the 10-minute mean wind speed, in both directions of $\beta = 0^o$ and $\beta = 90^o$. This is same as the conclusion made by Kato *et al.* (1991) in the full-scale measurement made on a 68 m high, 18 stories building in Yokohama, Japan.

6. Conclusions

The full-scale field measurements and wind tunnel test on wind-induced response of typical buildings in Singapore reveal that:

(1) Among the available empirical models in the literature for fundamental periods, the most appropriate model is the one proposed by Lagomarsino (1998). But yet a more accurate expressions for period of reinforced concrete building is proposed herein as:

$$T = H/53; \quad \text{for weaker axis}$$
$$T = H/68; \quad \text{for stronger axis}$$

(2) The infill walls contribute significantly to the stiffness during the wind induced excitations and therefore it is important to include their contribution for economical design under serviceability criteria which generally determine the member sizes for tall buildings.

(3) Comparison of wind-induced loads obtained from the wind tunnel with various codes reveal that the CP3 (1972) tends to give a good prediction on distribution of wind loads along the height of the building, while the Australian Code (2000) tends to be conservative for lower one-third of the building.

(4) The ratio between 3-second gust speed and 10-minute mean wind speed calculated from the field data is in good agreement with the values proposed by Deaves and Harries (Australian Standard 1989). The field measured turbulence spectra give a good agreement with the spectrum proposed by Von Karman (Scanlan and Simiu 1996).

(5) The field acceleration data for along and across wind compare well with AIJ [14]. The across wind acceleration data fall within the empirical range proposed by Vickery (1973). Whereas the RMS acceleration in along wind direction is accurately predicted by the Australian Code in terms of 3-second gust speed.

(6) The RMS accelerations for both wind tunnel test and field measurement increase in proportion to approximately the third power of the 10-minute mean wind speed, and both fall in line with AIJ (1996) prediction, this is in agreement with the finding by Kato *et al.* (1991).

Acknowledgements

The authors would like to express their gratitude to Engineer Lau Joo Ming and Engineer Chee Kheng Chye of the Housing Development Board, for their support that made this work possible.

References

Architectural Institute of Japan (1996), AIJ Recommendations for Loads on Buildings.
Australian/New Zealand Standard (2000), Structural Design- General Requirements and Deign Actions.
Australian Standard (AS 1170.2) (1989), Part 2: Wind Loads, Standard Australia, Australia.
Balendra, T., Kong, S.K., Shah, D.A. and Tey, K.L. (2002), "Evaluation of flow characteristics in the NUS-HDB wind tunnel", *J. Wind Eng. Ind. Aerodyn*., **90**, 675-688.
Balendra, T., Kong, S.K. and Tan, K.H. (1999), "Vulnerability of reinforced concrete frames in low seismic region, when designed according to BS8110", *Earthquake Eng. Struct. Dyn*., **28**, 1361-1381.
Balendra, T. (1993), *Vibration of Buildings to Wind and Earthquake Loads*, Springer- Verlag, London.
Brownjohn, J. (2001), Private Communication.
Casanova, D., Larose, G.L., Melelli, S. and Zasso, A. (1998), "Field measurements of the wind-induced response of a 254 m high free-standing bridge pylon", *J. Wind Eng. Ind. Aerodyn*., **74**, 891-902.
Clough, R.W. and Penzien, J. (1993), *Dynamics of Structure*, McGraw-Hill, NY.
Code of Basic Data for the Design of Buildings (1972), Chapter V: Loading, Part 2: Wind Loads, British Standard Institution, London.
Computers & Structures Inc. (1997), ETABS Three Dimensional Analysis of Building Systems, Berkeley, California, USA.
Ellis, B.R. (1998), "Full-scale measurements of dynamic characteristic of buildings in the UK", *J. Wind Eng. Ind. Aerodyn*., **59**, 365-382.
Fang, J.Q., Li, Q.S., Jeary, A.P. and Wong, C.K. (1998), "Full scale measurements of wind effects on tall buildings", *J. Wind Eng. Ind. Aerodyn*., **74**, 741-750.
Hong, L.L. and Hwang, W.L. (2000), "Empirical formula for fundamental vibration periods of reinforced concrete buildings in Taiwan", *Earthquake Engng Struct. Dyn*., **29**, 327-337.
International Conference of Building Officials (1997). Uniform Building Code (UBC). Whitterier, CA.
Kato, N., Marukawa, H., Niihori, Y. and Ohkuma, T. (1991), "Full-scale measurement of wind pressure and response accelerations of a high-rise building", *J. Wind Eng. Ind. Aerodyn*., **38**, 185-196.
Lagomarsino, S. (1998), "Forcast models for damping and vibration periods of buildings", *J. Wind Eng. Ind. Aerodyn*., **48**, 221-239.
Lyons, R.G. (1997), *Understanding Digital Signal Processing*, Addison-Westley Pub. Co.
Mainstone, R.J. (1974), "Supplementary note on the stiffness and strengths of infilled frames", Current Paper CP 13/74, Building Research Station, Garston, Watford.
Obasaju, E.D. (1992), "Measurement of forces and base overturning moments on the CAARC tall building model in a simulated atmospheric boundary layer", *J. Wind Eng. Ind. Aerodyn*., **40**, 103-126.
Ono, J., Sasaki, A. Satake, N. and Suda, K. (1998), "Damping properties of buildings in Japan", *J. Wind Eng. Ind. Aerodyn*., **59**, 383-392.
Scanlan, R.H. and Simiu, E. (1996), *Wind Effects on Structures*, 3rd edition, Wiley, New York.
Vickery, B.J. (1973), "Notes on wind forces on tall buildings", Annex to Australian Standard 1170, Part 2-1973, SAA Loading Code Part2- Wind Forces, Standards Association of Australia, Sydney.

Appendix

Vickery's across wind acceleration empirical formula

Vickery (1973) who has proposed the following empirical expression for the across-wind displacement and RMS acceleration:

$$\frac{\sigma_y(H)}{\sqrt{A}} = c\left[\frac{\bar{U}(H)}{n_1\sqrt{A}}\right]^{3.5} = \frac{1}{\sqrt{\zeta_1}}\frac{\rho}{\rho_b}$$

$$\sigma_{\ddot{y}}(H) = (2\pi n_1)^2\sigma_y(H)$$

where $\sigma_y(H)$: RMS tip displacement
H : height of the building
A : cross-sectional area of the building
$\bar{U}(H)$: the mean wind speed at the tip of the building
n_1 : the fundamental frequency of vibration
ζ : the damping ratio
ρ : the air density
ρ_b : the mass density of the building
c : determined empirically as 0.000015+/–0.00006

Wind-Induced Loads By CP3 (1972)

The wind force at every height level is given by:

$$F = C_f q A_e$$

where C_f = 0.97, obtained based on B/D and H/B ratio from Table 10 in CP3
B = breadth of the building, normal to wind stream
D = depth of the building, parallel to wind stream
H = height of the building
q = kV_s^2, dynamic pressure
k = 0.613 in SI units
V_s = $VS_1S_2S_3$

where V = taken as 33.3 m/s, basic wind speed, 3-second gust speed at 10 m above ground in open terrain, estimated to be exceed on the average once in 50 years
S_1 = 1, topography factor
S_2 = ground roughness, building size and height above ground factor, obtained from Table 3 in CP3 (1972)
S_3 = 1, statistical factor
A_e = the effective frontal area of the building at every height level.

CC